FERMILAB-PUB-04-326-E

Study of the $D^0 \to K^+K^-\pi^+\pi^-$ decay.

The FOCUS Collaboration

J. M. Link [a] P. M. Yager [a] J. C. Anjos [b] I. Bediaga [b] C. Göbel [b]
A. A. Machado [b] J. Magnin [b] A. Massafferri [b]
J. M. de Miranda [b] I. M. Pepe [b] E. Polycarpo [b] A. C. dos Reis [b]
S. Carrillo [c] E. Casimiro [c] E. Cuautle [c] A. Sánchez-Hernández [c]
C. Uribe [c] F. Vázquez [c] L. Agostino [d] L. Cinquini [d]
J. P. Cumalat [d] B. O'Reilly [d] I. Segoni [d] K. Stenson [d]
J. N. Butler [e] H. W. K. Cheung [e] G. Chiodini [e] I. Gaines [e]
P. H. Garbincius [e] L. A. Garren [e] E. Gottschalk [e] P. H. Kasper [e]
A. E. Kreymer [e] R. Kutschke [e] M. Wang [e] L. Benussi [f]
M. Bertani [f] S. Bianco [f] F. L. Fabbri [f] A. Zallo [f] M. Reyes [g]
C. Cawlfield [h] D. Y. Kim [h] A. Rahimi [h] J. Wiss [h] R. Gardner [i]
A. Kryemadhi [i] Y. S. Chung [j] J. S. Kang [j] B. R. Ko [j]
J. W. Kwak [j] K. B. Lee [j] K. Cho [k] H. Park [k] G. Alimonti [ℓ]
S. Barberis [ℓ] M. Boschini [ℓ] A. Cerutti [ℓ] P. D'Angelo [ℓ]
M. DiCorato [ℓ] P. Dini [ℓ] L. Edera [ℓ] S. Erba [ℓ] P. Inzani [ℓ]
F. Leveraro [ℓ] S. Malvezzi [ℓ] D. Menasce [ℓ] M. Mezzadri [ℓ]
L. Moroni [ℓ] D. Pedrini [ℓ] C. Pontoglio [ℓ] F. Prelz [ℓ] M. Rovere [ℓ]
S. Sala [ℓ] T. F. Davenport III [m] V. Arena [n] G. Boca [n]
G. Bonomi [n] G. Gianini [n] G. Liguori [n] D. Lopes Pegna [n]
M. M. Merlo [n] D. Pantea [n] S. P. Ratti [n] C. Riccardi [n] P. Vitulo [n]
H. Hernandez [o] A. M. Lopez [o] H. Mendez [o] A. Paris [o]
J. Quinones [o] J. E. Ramirez [o] Y. Zhang [o] J. R. Wilson [p]
T. Handler [q] R. Mitchell [q] D. Engh [r] M. Hosack [r] W. E. Johns [r]
E. Luiggi [r] J. E. Moore [r] M. Nehring [r] P. D. Sheldon [r]
E. W. Vaandering [r] M. Webster [r] M. Sheaff [s]

[a] *University of California, Davis, CA 95616*

[b] *Centro Brasileiro de Pesquisas Físicas, Rio de Janeiro, RJ, Brasil*

[c] *CINVESTAV, 07000 México City, DF, Mexico*

[d] *University of Colorado, Boulder, CO 80309*

[e] *Fermi National Accelerator Laboratory, Batavia, IL 60510*

[f] *Laboratori Nazionali di Frascati dell'INFN, Frascati, Italy I-00044*
[g] *University of Guanajuato, 37150 Leon, Guanajuato, Mexico*
[h] *University of Illinois, Urbana-Champaign, IL 61801*
[i] *Indiana University, Bloomington, IN 47405*
[j] *Korea University, Seoul, Korea 136-701*
[k] *Kyungpook National University, Taegu, Korea 702-701*
[ℓ] *INFN and University of Milano, Milano, Italy*
[m] *University of North Carolina, Asheville, NC 28804*
[n] *Dipartimento di Fisica Nucleare e Teorica and INFN, Pavia, Italy*
[o] *University of Puerto Rico, Mayaguez, PR 00681*
[p] *University of South Carolina, Columbia, SC 29208*
[q] *University of Tennessee, Knoxville, TN 37996*
[r] *Vanderbilt University, Nashville, TN 37235*
[s] *University of Wisconsin, Madison, WI 53706*
See http://www-focus.fnal.gov/authors.html for additional author information.

Abstract

Using data from the FOCUS (E831) experiment at Fermilab, we present a new measurement for the Cabibbo-suppressed decay mode $D^0 \to K^+K^-\pi^+\pi^-$. We measure:

$\Gamma(D^0 \to K^+K^-\pi^+\pi^-)/\Gamma(D^0 \to K^-\pi^-\pi^+\pi^+) = 0.0295 \pm 0.0011 \pm 0.0008\,.$

An amplitude analysis has been performed in order to determine the resonant substructure of this decay mode. The dominant components are the decays

$D^0 \to K_1(1270)^+K^-$, $D^0 \to K_1(1400)^+K^-$ and $D^0 \to \rho(770)^0\phi(1020)$.

1. Introduction

In recent years there has been a growing interest in multi-body hadronic decays of charm mesons. These decays provide a unique tool for investigating the weak decay of the charm quark in the environment of low energy strong interactions. High statistics data with small backgrounds are still dominated by three-body final states, but results on four-body final states are becoming available.

The picture emerging from many different Dalitz plot analyses reveals a rich resonant structure of these decays with a well defined pattern: final states that can proceed via simple spectator amplitudes in which the virtual W is coupled to a vector (V) or axial-vector (A) meson have large branching fractions compared to cases in which the W is coupled to a pseudoscalar (P) meson.

The decay mode $D^0 \to K^+K^-\pi^+\pi^-$ is Cabibbo-suppressed and may be produced through two and three-body intermediate resonant states. Following the above mentioned pattern, one expects dominant contributions from modes having the axial-vector mesons K_1 ($D \to AP$), namely $D^0 \to K_1(1270)^+K^-$ and $D^0 \to K_1(1400)^+K^-$, both resulting from W-radiation (spectator) amplitudes. Other tree-level amplitudes lead to intermediate two-body decays such as $D \to \phi(1020)\rho(770)^0$ ($D \to VV$), or even three-body decays like $D^0 \to \rho(770)^0K^+K^-$ ($D \to VPP$). The other possible contribution of the $D \to VV$ type comes from the mode $D^0 \to K^*(892)^0\bar{K}^*(892)^0$. In this case, however, there is no tree-level amplitude and the two W-exchange amplitudes cancel almost exactly in the SU(3) limit. This is an instance of a mode that should proceed primarily through final state interactions.

Most theoretical predictions of hadronic decay rates are still limited to Cabibbo favored modes and two-body decays. There are several predictions for the rate of the $D^0 \to \rho(770)^0\phi(1020)$ mode [1,2], but we are unaware of any prediction for $D^0 \to K_1^+K^-$.

In this paper we present a new measurement of the branching ratio $\Gamma(D^0 \to K^+K^-\pi^+\pi^-)/\Gamma(D^0 \to K^-\pi^-\pi^+\pi^+)$ using data from the FOCUS experiment. An amplitude analysis has been performed to determine the $D^0 \to K^+K^-\pi^+\pi^-$ resonant substructure.

FOCUS, an upgraded version of E687 [3], is a charm photoproduction experiment which collected data during the 1996–97 fixed target run at Fermilab. Electron and positron beams (typically with 300 GeV endpoint energy) obtained from the 800 GeV Tevatron proton beam produce, by means of bremsstrahlung, a photon beam which interacts with a segmented BeO target [4]. The mean photon energy for reconstructed charm events is ~ 180 GeV. A system of three multi-cell threshold Čerenkov counters performs the charged particle identification, separating kaons from pions up to a momentum of 60 GeV/c. Two systems of silicon microvertex detectors are used to track particles: the first system consists of 4 planes of microstrips interleaved with the experimental target [5] and the second system consists of 12 planes of microstrips located downstream of the target. These detectors provide high resolution in the transverse plane (approximately 9 μm), allowing the identification and separation of charm primary (production) and secondary (decay) vertices. The charged particle momentum is determined by measuring the deflections in two magnets of opposite polarity through five stations of multi-wire proportional chambers.

2. Analysis of the decay mode $D^0 \to K^+K^-\pi^+\pi^-$

The final states are selected using a candidate driven vertex algorithm [3]. A

secondary vertex is formed from the four candidate tracks. The momentum of the resultant D^0 candidate is used as a *seed* track to intersect the other reconstructed tracks and to search for a primary vertex. The confidence levels of both vertices are required to be greater than 1%. Once the production and decay vertices are determined, the distance L between the vertices and its error σ_L are computed. This is the most important variable for separating charm events from non-charm prompt backgrounds. Signal quality is further enhanced by cutting on *Iso2*. This isolation variable requires that all remaining tracks not assigned to the primary and secondary vertex have a confidence level smaller than the cut to form a vertex with the D candidate daughters. To minimize systematic errors on the measurements of the branching ratio, we use identical vertex cuts on the signal and normalizing mode, namely $L\,/\,\sigma_L > 9$ and $Iso2 < 10$ %. We also require the primary vertex to be formed with at least two reconstructed tracks in addition to the D^0 seed.

The only difference in the selection criteria between the $D^0 \to K^+K^-\pi^+\pi^-$ and $D^0 \to K^-\pi^-\pi^+\pi^+$ decay modes lies in the particle identification cuts. The Čerenkov identification cuts used in FOCUS are based on likelihood ratios between the various particle identification hypotheses. These likelihoods are computed for a given track from the observed firing response (on or off) of all the cells that are within the track's ($\beta = 1$) Čerenkov cone for each of our three Čerenkov counters. The product of all firing probabilities for all the cells within the three Čerenkov cones produces a χ^2-like variable $W_i = -2\ln(\text{Likelihood})$ where i ranges over the electron, pion, kaon, and proton hypotheses [6]. All kaon tracks are required to have $\Delta_K = W_\pi - W_K$ greater than 3 and all pion tracks are required to be separated by less than 5 units from the best hypothesis, that is $picon = W_{\min} - W_\pi$.

Using the set of selection cuts just described, we obtain the invariant mass distribution for $K^-K^+\pi^-\pi^+$ shown in Fig. 1a. Although the Čerenkov cuts considerably reduce the reflection peak (from $D^0 \to K^-\pi^+\pi^-\pi^+$) to the right of the signal peak, there is still a distortion of the background due to this surviving contamination. The shape of this reflection peak has been determined by generating Monte Carlo $D^0 \to K^-\pi^+\pi^-\pi^+$ events and reconstructing them as $K^-K^+\pi^-\pi^+$. The mass plot is fit with a function that includes two Gaussians with the same mean but different sigmas to take into account the variation in resolution vs. momentum of our spectrometer [3], a second-order polynomial for the combinatorial background and a shape for the reflection obtained by the Monte Carlo simulation. The amplitude of the reflection peak is a fit parameter while its shape is fixed. A log-likelihood fit gives a signal of 2669 ± 101 $K^-K^+\pi^-\pi^+$ events.

The large statistics $K^-\pi^-\pi^+\pi^+$ mass plot is fit with two Gaussians plus a second-order polynomial. The fit gives a signal of $131\,763 \pm 453$ $K^-\pi^-\pi^+\pi^+$ events.

The fitted D^0 masses are in good agreement with the world average [7] and the resolutions are in good agreement with those of our Monte Carlo simulation.

3. Relative Branching Ratio

The evaluation of relative branching ratios requires yields from the fits to be corrected for detector acceptance and efficiency. These differ among the various decay modes because of differences in both spectrometer acceptance (due to different Q values for the two decay modes) and Čerenkov identification efficiency.

From the Monte Carlo simulations, we compute the relative efficiencies to be: $\frac{\epsilon(D^0 \to K^+K^-\pi^+\pi^-)}{\epsilon(D^0 \to K^-\pi^-\pi^+\pi^+)} = 0.688 \pm 0.006$. Using the previous results, we obtain the following values for the branching ratio:

$$\Gamma(D^0 \to K^+K^-\pi^+\pi^-)/\Gamma(D^0 \to K^-\pi^-\pi^+\pi^+) = 0.0295 \pm 0.0011.$$

Our final measurements have been tested by modifying each of the vertex and Čerenkov cuts individually. The branching ratio is stable versus several sets of cuts as shown in Fig. 2. We varied the confidence level of the secondary vertex from 1% to 50%, *Iso2* from 10^{-6} to 1, $L\,/\,\sigma_L$ from 6 to 20, Δ_K from 1 to 5 and *picon* from -6 to -2 and consider the tight cut set used to study the sub-resonant structure (see below).

Systematic uncertainties on branching ratio measurements come from different sources. We consider four independent contributions to the systematic uncertainty: the *split sample* component, the *fit variant* component, the component due to the particular choice of the vertex and Čerenkov cuts (discussed previously), and the limited statistics of the Monte Carlo.

The *split sample* component takes into account the systematics introduced by a residual difference between data and Monte Carlo, due to a possible mismatch in the reproduction of the D^0 momentum and the changing experimental conditions of the spectrometer during data collection. This component has been determined by splitting data into four independent subsamples, according to the D^0 momentum range (high and low momentum) and the configuration of the vertex detector, that is, before and after the insertion of an upstream silicon system. A technique, employed in FOCUS and modeled after the *S-factor method* from the Particle Data Group [7], was used to try to separate true systematic variations from statistical fluctuations. The branching ratio is evaluated for each of the 4 ($= 2^2$) statistically independent subsamples and a *scaled error* $\tilde{\sigma}$ (that is the errors are boosted when $\chi^2/(N-1) > 1$) is calculated. The *split sample* error $\sigma_{\rm split}$ is defined as the difference between the reported statistical error and the scaled error, if the scaled error exceeds the statistical error [8].

Source	Systematic error
Split sample	0.0%
Fit Variant	2.1%
Set of cuts	1.7%
MC statistics	0.9%
Total systematic error	2.8%

Table 1
Contribution in percent to the systematic uncertainties of the branching ratio $\Gamma(D^0 \to K^-K^+\pi^-\pi^+)/\Gamma(D^0 \to K^-\pi^-\pi^+\pi^+)$.

Another possible source of systematic uncertainty is the *fit variant*. This component is computed by varying, in a reasonable manner, the fitting conditions for the whole data set. In our study we fixed the widths of the Gaussians to the values obtained by the Monte Carlo simulation, we changed the background parametrization (varying the degree of the polynomial), we removed the reflection peak from the fit function, and we use one Gaussian instead of two. Finally the variation of the computed efficiencies, both for $D^0 \to K^-K^+\pi^+\pi^-$ and the normalizing decay mode, due to the different resonant substructure simulated in the Monte Carlo has been taken into account. The BR values obtained by these variants are all *a priori* equally likely, therefore this uncertainty can be estimated by the *r.m.s.* of the measurements [8].

Analogously to the *fit variant*, the cut component is estimated using the standard deviation of the several sets of cuts shown in Fig. 2. Actually this is an overestimate of the cut component because the statistics of the cut samples are different.

Finally, there is a further contribution due to the limited statistics of the Monte Carlo simulation used to determine the efficiencies. Adding in quadrature the four components, we get the final systematic errors which are summarized in Table 1.

The final result is shown in Table 2 along with a comparison with the previous determinations.

4. Amplitude analysis of $D^0 \to K^+K^-\pi^+\pi^-$

A fully coherent amplitude analysis was performed in order to determine the resonant substructure of the $D^0 \to K^+K^-\pi^+\pi^-$ decay. Previous results on this mode were obtained from small samples. E687 [10] did an incoherent analysis, while the analysis of E791 [9] quoted only inclusive fractions.

Experiment	$\frac{\Gamma(D^0\to K^+K^-\pi^+\pi^-)}{\Gamma(D^0\to K^-\pi^-\pi^+\pi^+)}$	Events
FOCUS (this result)	$0.0295 \pm 0.0011 \pm 0.0008$	2669 ± 101
E791 [9]	$0.0313 \pm 0.0037 \pm 0.0036$	136 ± 15
E687 [10]	$0.035 \pm 0.004 \pm 0.002$	244 ± 26
ARGUS [11]	$0.041 \pm 0.007 \pm 0.005$	114 ± 20
CLEO [12]	$0.0314 \pm 0.010 \pm 0.005$	89 ± 29

Table 2
Comparison with other experiments.

Tighter cuts have been applied in the selection of events for the amplitude analysis. We require: $L\,/\,\sigma_L > 10$, secondary CL > 0.05, $\Delta_K > 4$, $Iso2 < 10^{-5}$. In addition the secondary vertex must lie outside of the segmented targets to reduce contamination due to secondary interactions. Using this set of cuts we obtain the invariant mass distribution shown in Fig. 1b. The mass plot is fit with a function that includes two Gaussians, a second-order polynomial for the combinatorial background, and a shape for the reflection peak (similar to the fit of Fig. 1a). A log-likelihood fit finds 1279 ± 48 $K^-K^+\pi^-\pi^+$ signal events.

Figure 3 shows the K^-K^+, $K^-\pi^+$, and $\pi^-\pi^+$ projections. We observe clear signals of the $\phi(1020)$, $\rho(770)^0$ and $K^*(892)^0$. These signals could come from decays of the axial-vector mesons $K_1(1270)^+$ and $K_1(1400)^+$, or from decays of the type $D^0 \to VV$ and $D^0 \to VPP$ ($V = \phi(1020)$, $\rho(770)^0$, $K^*(892)^0$, $P = \pi^\pm, K^\pm$). The $K_1(1270)^+$ decay modes that lead to a $K^-K^+\pi^-\pi^+$ final state are $\rho(770)^0K^+$, $K^*(892)^0\pi^+$, $K_0^*(1430)\pi^+$ and ωK^+, whereas the $K_1(1400)^+$ decays only to $K^*(892)^0\pi^+$. The ωK^+ mode is not considered because the branching fraction of $\omega \to \pi^+\pi^-$ is less than 2%. These components are distinguishable by the characteristic angular distributions of the final state particles.

In our model we consider two $D \to AP$ modes, $K_1(1270)^+K^-$ and $K_1(1400)^+K^-$. We also consider contributions from two $D \to VV$ modes, $\phi(1020)\rho(770)^0$ and $K^*(892)^0\bar{K}^*(892)^0$, and from three $D \to VPP$ modes, $\rho(770)^0K^+K^-$, $\phi(1020)\pi\pi$, and $K^*(892)^0K^+\pi^-$. Finally, we include the mode $f_0(980)\pi^+\pi^-$ ($D \to SPP$), since the $f_0(980)$ has a strong coupling to the K^+K^- channel. The mode $f_0(980)K^+K^-$ is not considered because there is no phase space for it. In principle the mode $a_0(980)\pi^+\pi^-$ could also contribute, but with the present statistics one cannot distinguish between the $a_0(980)$ and $f_0(980)$. Moreover, the dominant component of the $a_0(980)$ is the $\eta\pi$ channel. A good description of our data is obtained without the non-resonant channel.

The formalism used in this amplitude analysis is a straightforward extension to four-body decays of the usual Dalitz plot fit technique. The overall signal

amplitude is a coherent sum of the ten individual amplitudes, $\mathcal{A} = \sum_k c_k A_k$. The amplitudes A_k are constructed as a product of form factors, relativistic Breit-Wigner functions, and spin amplitudes which account for angular momentum conservation. We use the Blatt-Weisskopf damping factors [13], F_l, as form factors (l is the orbital angular momentum of the decay vertex). For the spin amplitudes we use the Lorentz invariant amplitudes [14], which depend both on the spin of the resonance(s) and the orbital angular momentum. The relativistic Breit-Wigner is

$$BW = \frac{1}{m^2 - m_0^2 + im_0\Gamma(m)},$$

where

$$\Gamma(m) = \Gamma_0 \frac{m_0}{m} \left(\frac{p^*}{p_0^*}\right)^{2s+1} \frac{F_l^2}{F_{l0}^2}.$$

In the above equations, m is the two-body invariant mass, m_0 is the resonance nominal mass, and $p^* = p^*(m)$ is the breakup momentum at resonance mass m.

Masses and widths of resonances are taken from the PDG [7], except for the $\rho(770)^0$ and the $f_0(980)$. The line shape of the $\rho(770)^0$ is taken from Crystal Barrel [15], and includes the $\rho - \omega$ interference. This significantly improves the fit. For the $f_0(980)$ we used the Flatte formula [16] of a coupled channel Breit-Wigner function. The $f_0(980)$ parameters — $g_\pi = 0.20 \pm 0.04$, $g_K = 0.50 \pm 0.20$ and $m_0 = (0.957 \pm 0.008)\mathrm{GeV}/c^2$ — are obtained by a fit to the FOCUS $D_s^+ \to \pi^+\pi^-\pi^+$ Dalitz plot, where the $f_0(980)\pi^+$ is the dominant component. Magnitudes and phases of the $K_1(1270)^+$ decay modes relative to the $\rho(770)^0 K^+$ were determined by the fit, since the limited D^0 phase space will affect the $K_1(1270)^+$ decay fractions.

The fit parameters are the 9 complex coefficients c_k. Magnitudes and phases are relative to those of the chain $D^0 \to K_1(1270)^+ K^-, K_1(1270)^+ \to \rho(770)^0 K^+$. The overall signal amplitude is corrected on an event-by-event basis for the acceptance, which is nearly constant across the phase space. The finite detector resolution causes a smearing of the edges of the five-dimensional phase space. This effect is taken into account by multiplying the overall signal distribution by a Gaussian factor, $g(M)$ (M being the $K^+K^-\pi^+\pi^-$ mass). The normalized signal probability distribution is, thus,

$$P_S(\phi) = \frac{1}{N_S} \varepsilon(\phi)\rho(\phi)g(M) \left|\sum c_k A_k(\phi)\right|^2$$

with ϕ being the coordinates of an event in the five dimensional phase space,

$\varepsilon(\phi)$ the acceptance function, and $\rho(\phi)$ the phase space density.

We consider four types of background events: random combinations of a $\phi(1020)$ and a $\pi^-\pi^+$ pair, a $K^*(892)^0$ plus a $K^-\pi^+$ pair, a $\rho(770)^0$ plus a K^+K^- pair, and random combinations of $K^+K^-\pi^+\pi^-$. The relative fractions of these backgrounds were determined from a fit to the data on the side bands of the $K^+K^-\pi^+\pi^-$ mass spectrum. This fit yields 69% for random combinations of $K^+K^-\pi^+\pi^-$. The fractions of the $\phi(1020)\pi^+\pi^-$, $K^*(892)^0K^-\pi^+$, and $\rho(770)^0K^+K^-$ backgrounds are 17%, 5% and 9%, respectively.

We assume the random $K^+K^-\pi^+\pi^-$ combinations to be uniformly distributed in phase space, whereas for the other backgrounds we assume Breit-Wigners with no form factors and no angular distribution. The overall background distribution is a weighted, incoherent sum of the four components described above. The relative background fractions, b_k, are fixed in the fit. The overall background distribution is also corrected for the acceptance (assumed to be the same as for the signal events) on an event-by-event basis and multiplied by an exponential function $b(M)$, accounting for the $K^+K^-\pi^+\pi^-$mass distribution of the background. The normalized background probability distribution is

$$P_B(\phi) = \frac{1}{N_B}\varepsilon(\phi)\rho(\phi)b(M)\sum b_k B_k(\phi).$$

An unbinned maximum likelihood fit was performed, minimizing the quantity $w \equiv -2\ln(\mathcal{L})$. The likelihood function, $\mathcal{L}$, is

$$\mathcal{L} = \prod_{\text{events}} \left[P_S(\phi^i) + P_B(\phi^i)\right].$$

Decay fractions are obtained from the coefficients c_k, determined by the fit, and after integrating the overall signal amplitude over the phase space [17]. Errors on the fractions include errors on both magnitudes and phases, and are computed using the full covariance matrix.

The result from the best fit is shown in Table 3. The dominant component is indeed the mode $D^0 \to K_1^+(1270^+)K^-$, with a fraction of $(33 \pm 6 \pm 4)\%$. Integrating the amplitude squared for the summed $D \to AP$ components gives nearly 55% of the total decay rate. This result is consistent with other D decays, for instance, the case of $D^0 \to K^-\pi^+\pi^-\pi^+$, which is dominated by the mode $a_1(1260)^+K^-$ with a fraction of about 50%.

The second dominant component is the $D \to VV$ mode: a large contribution of the $\phi(1020)\rho(770)^0$ channel, with a fraction of 29%, and a small, but significant, contribution from $K^*(892)^0\bar{K}^*(892)^0$. The $\phi(1020)\rho(770)^0$ channel can proceed through an internal W radiation amplitude, while the $K^*(892)^0\bar{K}^*(892)^0$

results from final state interactions. Using the value of $\Gamma(D^0 \to K^+K^-\pi^+\pi^-)/\Gamma(D^0 \to K^-\pi^-\pi^+\pi^+)$ we measured, we obtain $B(D^0 \to \phi(1020)\rho(770)^0) = (1.2 \pm 0.1) \times 10^{-3}$. This is a factor of five higher than the prediction of Bedaque, Das and Mathur [2], $(B(D^0 \to \phi(1020)\rho(770)^0) = 2.2 \times 10^{-4})$. The model of Bauer, Steck and Wirbel [1] predicts $B(D^0 \to \phi(1020)\rho(770)^0) = 4.5 \times 10^{-3}$, which is a factor of 3.5 higher than our value.

Finally, the remaining fraction comes from the $D \to VPP$ and $D \to SPP$ decays. Altogether, these modes account for nearly 30% of the total decay rate. A similar result was found in our analysis of the $D^0 \to K^+K^-K^-\pi^+$ decay [17], showing the importance of the three-body channels in four-body decays of D mesons. In addition to the three $D \to VPP$ modes listed above, we have also included the mode $K^*(1400)^+K^-$, but its contribution is negligible.

The K^+K^- spectrum has an interesting feature. Near the threshold it is dominated by the $\phi(1020)$ peak, but the $\phi(1020)$ line shape is distorted by the presence of the $f_0(980)$. The $\phi(1020)$ and $f_0(980)$ cannot be distinguished with purely a mass cut on K^+K^- invariant mass. The fairly large fraction (15%) of the $D^0 \to f_0(980)\pi^+\pi^-$ mode shows that the $f_0(980)$ contribution cannot be neglected. The distinction between $\phi(1020)$ and $f_0(980)$ components requires a full angular analysis.

In four body decays the phase space is 5-dimensional, so we can only look at projections. In Figure 4, the K^+K^-, $\pi^+\pi^-$, and $K^-\pi^+$ invariant mass projections of events used in the amplitude analysis are superimposed on the fit result, with the background projections shown in the shaded histograms. The fit result can also be displayed in two dimensional projections, shown in Figure 5, and in distributions of the cosine of helicity and acoplanarity angles, shown in Figure 6. In the case of the $D^0 \to \phi(1020)\rho(770)^0$ mode, the helicity angle is defined as the angle between the K^- (π^-) and the direction of the recoiling $\rho(770)^0$ ($\phi(1020)$) in the $\phi(1020)$ ($\rho(770)^0$) rest frame. In the case of $D^0 \to K^*(892)^0\bar{K}^*(892)^0$, helicity angles are defined as the angle between the K and the recoiling $K^*(892)^0$ in each $K^*(892)^0$ frame. The acoplanarity angle is the angle between the $\phi(1020)$ and $\rho(770)^0$ decay planes, measured in the D rest frame. The bump in the central part of the $\rho(770)^0$ helicity angle distribution is due to the decay chain $D^0 \to K_1(1270)^+K^-$, $K_1(1270)^+ \to \rho(770)^0K^+$.

The goodness-of-fit was assessed using a χ^2 test. The five invariants used to define the kinematics of this decay are the K^-K^+, $\pi^+\pi^-$, $K^-\pi^+$, $K^+\pi^-$ and $K^-\pi^-$ masses squared. Due to the limited statistics we have integrated over the latter invariant and divided the other four into three bins each, yielding a total of 45 cells. Data and Monte Carlo samples were divided into these 45 cells. The fit has 18 free parameters, so the number of degrees of freedom is $45 - 18 = 27$. We obtain a χ^2 of 40.4, and from this value the estimated

Mode	Magnitude	Phase	Fraction (%)
$K_1(1270)^+K^-,\ K_1 \to \rho(770)^0K^+$	1 (fixed)	0 (fixed)	$18 \pm 6 \pm 3$
$K_1(1270)^+K^-,\ K_1 \to K_0^*(1430)\pi^+$	$0.27 \pm 0.08 \pm 0.06$	$354 \pm 19 \pm 19$	$2 \pm 1 \pm 0$
$K_1(1270)^+K^-,\ K_1 \to K^*(892)^0\pi^+$	$0.94 \pm 0.16 \pm 0.13$	$12 \pm 12 \pm 15$	$16 \pm 4 \pm 5$
$K_1(1270)^+K^-$, (all modes)	—	—	$33 \pm 6 \pm 4$
$K_1(1400)^+K^-$	$1.18 \pm 0.19 \pm 0.09$	$259 \pm 11 \pm 13$	$22 \pm 3 \pm 4$
$K^*(892)0\bar{K}^*(892)^0$	$0.39 \pm 0.09 \pm 0.11$	$28 \pm 13 \pm 10$	$3 \pm 2 \pm 1$
$\phi(1020)\rho(770)^0$	$1.30 \pm 0.11 \pm 0.07$	$49 \pm 11 \pm 12$	$29 \pm 2 \pm 1$
$\rho(770)^0K^+K^-$	$0.33 \pm 0.12 \pm 0.16$	$278 \pm 26 \pm 20$	$2 \pm 2 \pm 2$
$\phi(1020)\pi^+\pi^-$	$0.30 \pm 0.06 \pm 0.06$	$163 \pm 16 \pm 15$	$1 \pm 1 \pm 0$
$K^*(892)^0K^+\pi^-$	$0.83 \pm 0.09 \pm 0.10$	$234 \pm 10 \pm 11$	$11 \pm 2 \pm 1$
$f_0(980)\pi^+\pi^-$	$0.91 \pm 0.13 \pm 0.05$	$240 \pm 11 \pm 17$	$15 \pm 3 \pm 2$

Table 3
Results from the best fit. The second error on the fractions, magnitudes and phases is systematic. The fraction for the mode $K_1(1270)^+K^-$ (fourth row) includes all three decay modes of the $K_1(1270)^+$, added coherently.

confidence level of the fit was 4.7%.

We consider three different sources of systematic uncertainties for the amplitudes analysis: *split sample*, using the same subsamples described previously, *fit variant*, varying the fitting conditions of the whole data set and the component due to the particular choice of the vertex and Čerenkov cuts. The most important contributions from *fit variant* systematic errors are: parameterization of the $f_0(980)$ line shape, uncertainty in the relative background fractions, and uncertainty in the masses and widths of the resonances. We have also considered the effect of ignoring form factors and using a flat acceptance. The cut component systematic errors were estimated using the standard deviation of several different sets of vertex/particle identification cuts, as we did in the branching ratio measurement. Systematic errors on phases and fractions were obtained adding in quadrature the *split sample*, *fit variant*, and cut component errors.

5. Conclusions

Using data from the FOCUS (E831) experiment at Fermilab, we studied the Cabibbo-suppressed decay mode $D^0 \to K^+K^-\pi^+\pi^-$.

A comparison with the two previous determinations of the relative branching ratio $\Gamma(D^0 \to K^+K^-\pi^+\pi^-)/\Gamma(D^0 \to K^-\pi^-\pi^+\pi^+)$ shows an impressive improvement in the accuracy of this measurement.

A coherent amplitude analysis of $K^+K^-\pi^+\pi^-$ final states was performed, showing that the dominant contribution comes from $D^0 \to AP$ modes, corresponding to nearly 55% of the $D^0 \to K^+K^-\pi^+\pi^-$ decay rate. We also measured an important contribution from D^0 decaying to two vector mesons, corresponding to nearly 30% of the decay rate. The remaining fraction of the $D^0 \to K^+K^-\pi^+\pi^-$ decay rate comes from decays of the type $D^0 \to VPP$ and $D^0 \to SPP$, with important contributions from $K^*(892)^0K^-\pi^+$ and $f_0(980)\pi^+\pi^-$.

We wish to acknowledge the assistance of the staffs of Fermi National Accelerator Laboratory, the INFN of Italy, and the physics departments of the collaborating institutions. This research was supported in part by the U. S. National Science Foundation, the U. S. Department of Energy, the Italian Istituto Nazionale di Fisica Nucleare and Ministero della Istruzione Università e Ricerca, the Brazilian Conselho Nacional de Desenvolvimento Científico e Tecnológico, CONACyT-México, and the Korea Research Foundation of the Korean Ministry of Education.

References

[1] M. Bauer, B. Steck and M. Wirbel, Z. Phys. C 34 (1987) 103.

[2] P. Bedaque, A. Das and V.S. Mathur, Phys. Rev. D 49 (1994) 269.

[3] E687 Collaboration, P.L. Frabetti *et al.*, Nucl. Instrum. Meth. A 320 (1992) 519.

[4] E687 Collaboration, P.L. Frabetti *et al.*, Nucl. Instrum. Meth. A 329 (1993) 62.

[5] FOCUS Collaboration, J.M. Link *et al.*, Nucl. Instrum. Meth. A 516(2004) 364.

[6] FOCUS Collaboration, J.M. Link *et al.*, Nucl. Instrum. Meth. A 484 (2002) 270.

[7] S. Eidelman *et al.* (Particle Data Group), Phys. Lett. B 592 (2004), 1.

[8] FOCUS Collaboration, J.M. Link *et al.*, Phys. Lett. B 555 (2003) 173.

[9] E791 Collaboration, E.M. Aitala *et al.*, Phys. Lett. B 423 (1998) 185.

[10] E687 Collaboration, P.L. Frabetti *et al.*, Phys. Lett. B 354 (1995) 486.

[11] ARGUS Collaboration, H. Albrecht *et al.*, Z.Phys. C 64 (1994) 375.

[12] CLEO Collaboration, R. Ammar *et al.*, Phys. Rev. D 44 (1991) 3383.

[13] J.M. Blatt and V.F. Weisskopf, *Theoretical Nuclear Physics*, John Wiley & Sons, New York, 1952.

[14] MARKIII Collaboration, D. Coffman *et al.*, Phys. Rev. D 45 (1992) 2196.

[15] Crystal Barrel Collaboration, A. Abele *et al.*, Phys. Lett. B 411 (1997) 354.

[16] S.M. Flatte, Phys. Lett. B 63 (1976) 228.

[17] FOCUS Collaboration, J.M. Link *et al.*, Phys. Lett. B 575 (2003) 190.

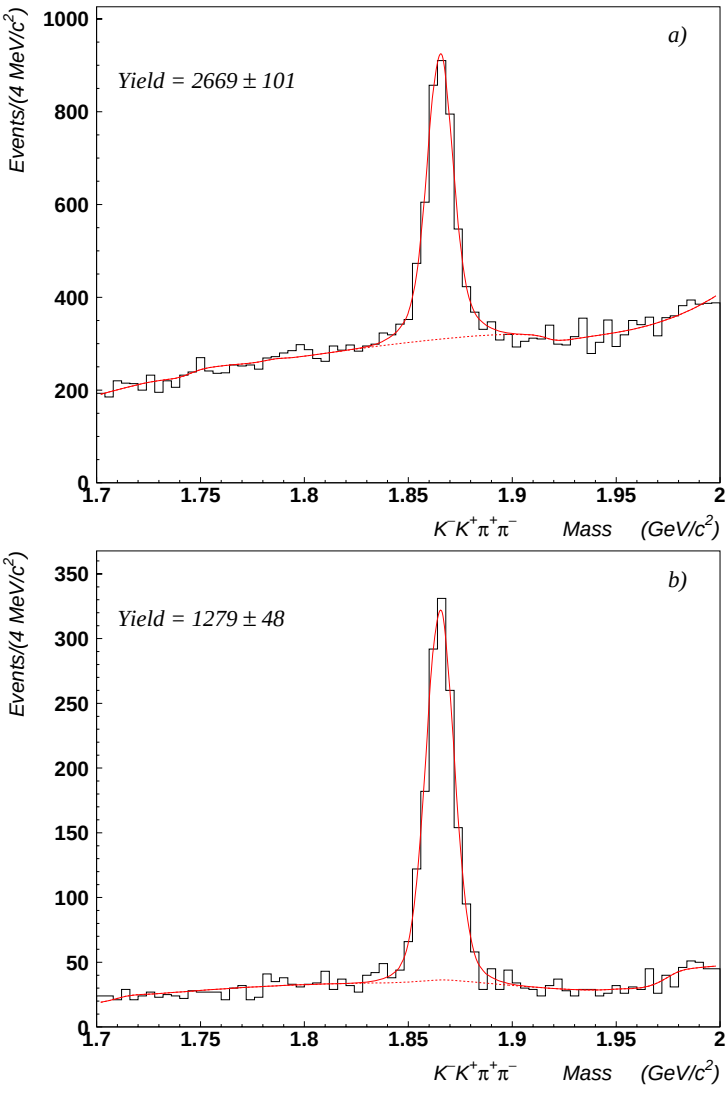

Fig. 1. Invariant mass distributions for $K^-K^+\pi^-\pi^+$ with standard cuts (a) used to determine the BR and tight cuts (b) used to study the subresonant structure. The fit (solid curve) is explained in the text, the dashed line shows the background

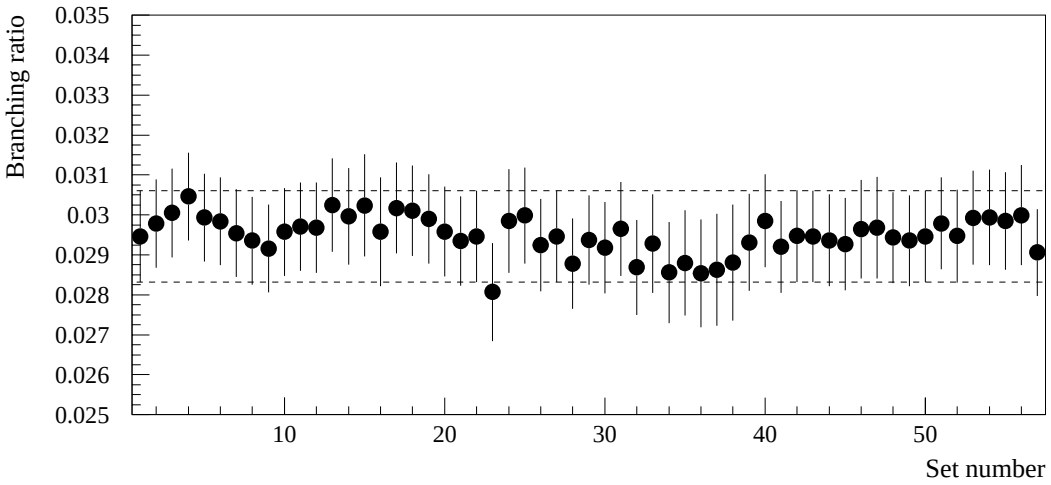

Fig. 2. Branching ratio $\Gamma(D^0 \to K^- K^+ \pi^- \pi^+)/\Gamma(D^0 \to K^- \pi^- \pi^+ \pi^+)$ versus several sets of cuts. We varied the confidence level of the secondary vertex from 1% to 50% (16 points), *Iso2* from 10^{-6} to 1 (7 points), $L\,/\,\sigma_L$ from 6 to 20 (15 points), Δ_K from 1 to 5 (9 points), *picon* from -6 to -2 (9 points), and finally we consider the tight cut set used to study the subresonant structure (last point). The dashed lines show the quoted branching ratio $\pm 1\sigma$.

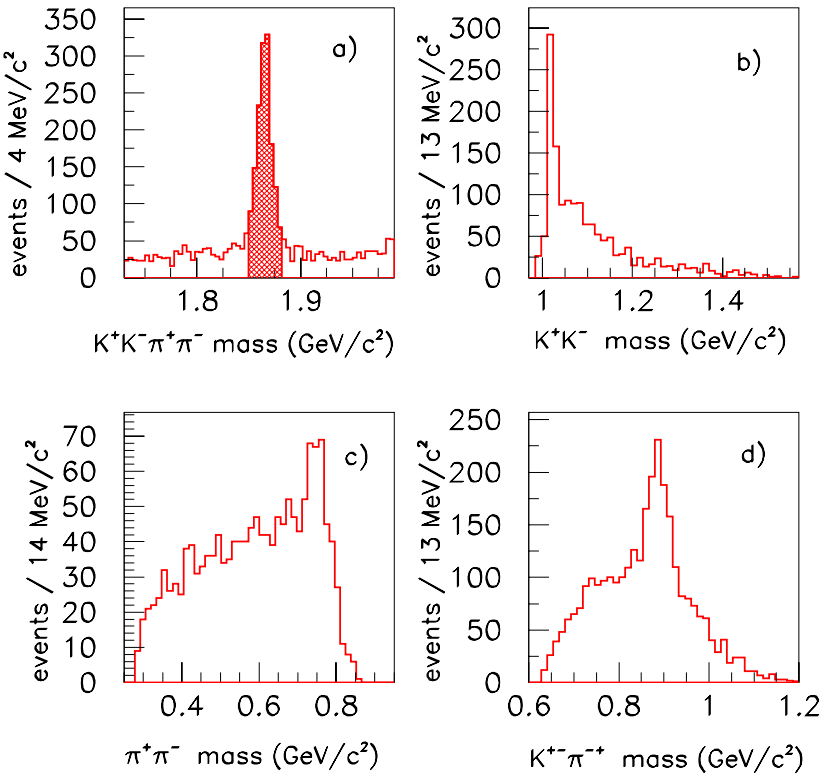

Fig. 3. a) The $K^+K^-\pi^-\pi^+$ mass plot with tight cuts. The hatched area corresponds to the events used in the amplitude analysis. The other plots show two-body projections of these events: b) K^+K^-; c) $\pi^-\pi^+$; d) $K^+\pi^-$ plus $K^-\pi^+$ (two independent entries per event). We observe clear signals of $\phi(1020)$, $\rho(770)^0$ and $K^{*0}(892)$.

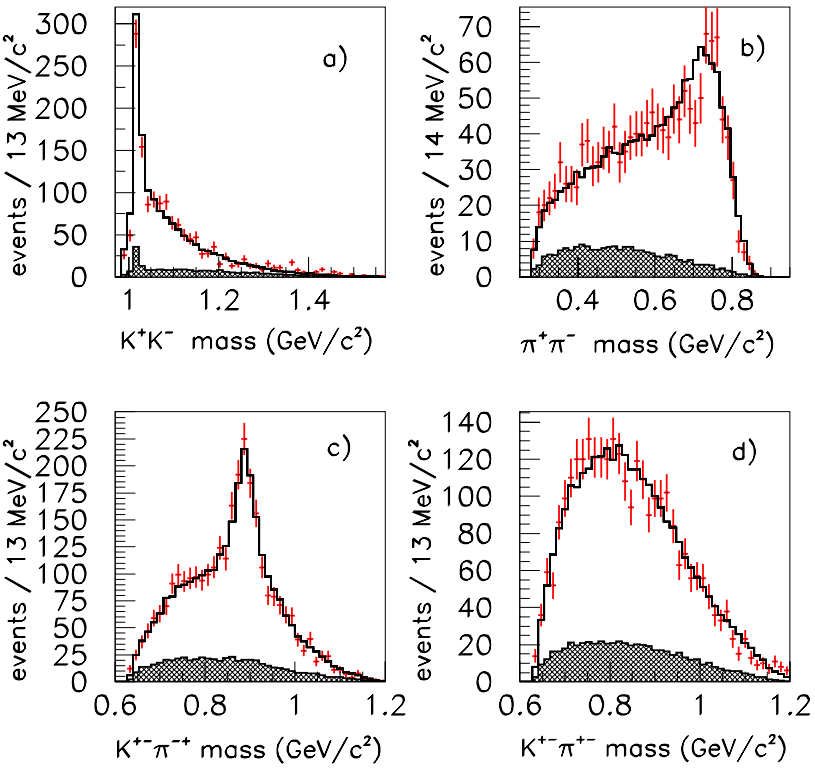

Fig. 4. The two-body projections with the fit result (solid line) and background (shaded histogram) superimposed: a) K^+K^-; b) $\pi^-\pi^+$; c) $K^+\pi^-$ plus $K^-\pi^+$ (two entries per event); d) $K^+\pi^+$ plus $K^-\pi^-$ (two entries per event).

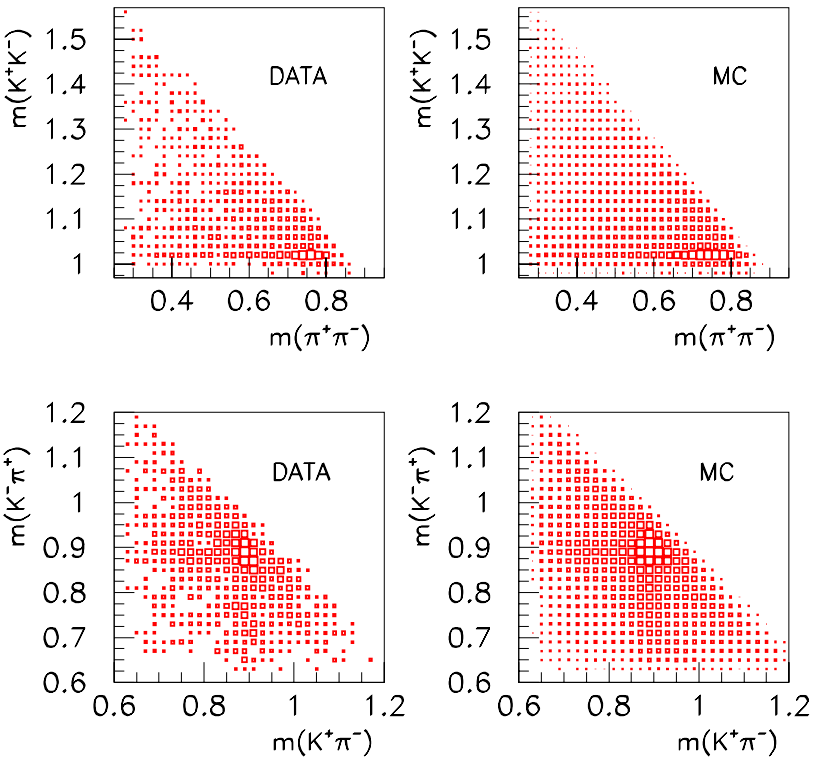

Fig. 5. Two-dimensional projections: K^+K^- *vs.* $\pi^-\pi^+$ in the top row, $K^+\pi^-$ *vs.* $K^-\pi^+$ in the lower row. Data is in the left column; mini-MC, generated according to the fit solution, is in the right column.

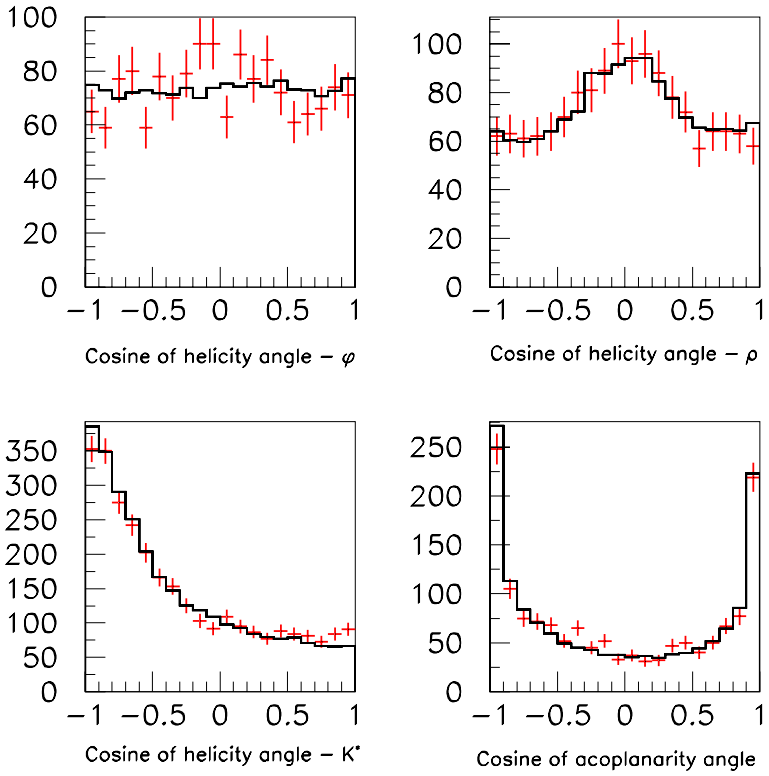

Fig. 6. Distribution of cosine of the helicity and acoplanarity angles (see text for angle definitions) The bump in the central part in the distribution of cosine of ρ helicity angle (top right plot) is caused by the chain $D^0 \to K_1(1270)K$, $K_1(1270) \to \rho K$.